Upregulation of phosphoglyceric acid mutase (PGAM)-1 is related to lymph node metastasis in gastric cancer

Helei Wang
The First Hospital of Jilin University
Daguang Wang
The First Hospital of Jilin University
Zhicheng Liu
The First Hospital of Jilin University
Lei Wang
The First Hospital of Jilin University
Zitian Wang
David Geffen School of Medicine at UCLA
Nicholas A. Cacalano (ncacalan@ucla.edu)
David Geffen School of Medicine at UCLA
Jian Suo
The First Hospital of Jilin University

Research Article

Keywords: gastric cancer (GC), lymph node metastasis, phosphoglyceric acid mutase-1 (PGAM1), Src/FAK/Paxillin pathway

Posted Date: June 7th, 2022

DOI: https://doi.org/10.21203/rs.3.rs-1720603/v1

Abstract

BACKGROUND: Gastric cancer (GC) is the most common malignancy of the digestive system, causing over two hundred thousand deaths annually in China and over 750,000 deaths worldwide. The high invasiveness and metastatic rates are mainly responsible for mortality due to GC. Thus, it is an urgent priority to explore the mechanisms underlying GC metastasis to improve cancer diagnosis develop more effective biological targeting agents.

METHODS: High-throughput RNA sequencing, quantitative PCR (q-PCR) and immunohistochemistry were used to compare PGAM1 levels in lymph node metastasis (LNM) tissues and carcinoma *in situ* (CIS) and noncancerous tissues from GC patients and correlated PGAM1 expression with patient prognosis, disease recurrence and mortality. In two GC cell lines (SGC7901 and BGC823) with sh-RNA-mediated PGAM1 knockdown, we analyzed cell growth *in vitro*, apoptosis and cell cycle progression by flow cytometry, and cell migration in wound-healing studies and transwell assays. *In vivo* subcutaneous growth of control and PGAM1 knockdown GC cell lines was measured in immunodeficient mice, and the potential role of PGAM1 in the expression of metastatic proteins and activation of migratory signaling was determined by flow cytometry and phospho-western blot analysis.

RESULTS: We found that elevated PGAM1 expression in LNM, but not CIS tissues correlated with increased disease recurrence and death of GC patients. PGAM1 knockdown impaired proliferation, cell cycle progression and migration of GC cell lines. In a murine xenograft model, GC cells with a PGAM1 knockdown displayed decreased growth capacity *in vivo* relative to control cells. Western blot and flow cytometry analysis showed that PGAM1 knockdown in SGC7901 and BGC823 decreased the expression of metalloproteinases MMP2 and MMP9 as well as the adhesion molecule ICAM-I, and impaired phosphorylation of Src, FAK and Paxillin relative to parental cells.

CONCLUSIONS: Our results indicate that PGAM1 is a novel biomarker of metastatic GC and may play an important role in promoting GC lymph node metastasis by driving cell proliferation, activating cytoskeletal reorganization and cell migration through the Src/FAK/Paxillin pathway and promoting digestion of the extracellular matrix by upregulating the expression of MMP2 and MMP9.

Introduction

Gastric cancer (GC) is the most common malignancy of the digestive system. In 2018, there were over 1 million new GC cases which resulted in approximately 8.2% of total cancer-related deaths worldwide [1]. GC also has a high incidence in China, and over two hundred thousand patients are projected to die annually from gastric cancer [2]. Clinical studies revealed that invasion and migration of tumor cells are the pivotal causes behind the high mortality rate of GC [3], yet the molecular basis of GC invasiveness and metastasis remains obscure. Despite the application of many traditional therapeutic modalities, including surgery, radiotherapy, and chemotherapy for the treatment of GC, the overall prognosis of

advanced GC patients is still [4–5]. Thus, it is an urgent priority to identify the mechanisms underlying the high rate of GC metastasis, and to exploit novel findings for therapeutic benefit.

Phosphoglycerate mutase 1 (PGAM1) is a key enzyme in the conversion of 3-phosphoglycerate (3-PG) into 2-phosphoglycerate (2-PG) during glycolysis [6]. Previous studies have shown that PGAM1 expression is upregulated in several types of cancers such as hepatocellular carcinoma [7], colorectal cancer [8], oral squamous cell carcinoma [9], non-small cell lung cancer [10], bladder cancer [11], renal clear cell carcinoma [12] and astrocytoma [13]. Meanwhile, the functions of PGAM1 in promoting tumor growth and migration have been described in several tumor cell lines [14–15] and in breast cancer models [16]. The role of PGAM1 in gastric cancer, however, remains understudied and poorly understood.

In this work, the mRNA profile of GC lymph node metastasis (LNM) tissues and GC carcinoma *in situ* (CIS) tissues was examined by high-throughput RNA sequencing. PGAM1 expression was found to be significantly up-regulated in LNM tissue compared to CIS tissues. In addition, PGAM1 over-expression was confirmed by q-PCR and IHC in clinical samples (n = 56). To further elucidate the function of PGAM1 in GC, we identified the roles of PGAM1 in the growth, cell cycle, apoptosis and migration of two independent PGAM1 knockdown GC cell lines which are representative of lymph node metastatic (SGC7901) or non-metastatic gastric cancer (BGC823). The growth rate of both PGAM1 knockdown GC cell lines was further examined in a murine GC xenograft model. Finally, the potential key signal proteins involved in PGAM1 related metastasis process were also identified.

Materials And Methods

Patient Samples

Three patients diagnosed with gastric cancer were enrolled in a mRNA sequencing group, and fifty-six GC patients were enrolled in an expanded group as verification samples. All patients received radical gastrectomy for gastric cancer in the First Hospital of Jilin University between 2017-2018. Paracancerous tissues, CIS tissues and LNM tissues were obtained by microdissection of frozen thin sections. The backgrounds and clinicopathological characteristics of patients in the sequencing group are summarized in table 1. The information of patients in the expanded group is shown in supplementary materials (supplementary table 1).

Two years after surgery, all patients were followed up by telephone interviews. The follow-up data were recorded as survival (0 points), death (1 point), lost/missing data (2 points), and recurrence (3 points). This study was approved by the Ethics Committees of the First Hospital of Jilin University. The ethics form and signed informed consent from all patients are shown in the supplementary materials.

Microdissection of tumor tissue and RNAsequencing

Surgical samples were embedded in OCT and sliced by freezing microtome. The slices were fixed in 95% ethanol for 2 min and stained with haematine for 30 seconds. After washing with ddH_2O containing 1‰

DEPC, tissue slices were microdissected using laser capture microdissection, equipped with a 355 nm ultraviolet laser diode (LMD6000, Leica Microsystems, Buffalo Grove, IL). Total RNA was isolated from dissected tissues using the PicoPure protocol (Arcturus, Mountain View, CA). The mRNA was amplified with two linear amplification steps by *in vitro* transcription using the MEGAscript T7 kit (Ambion, Austin, TX), followed by the labeling step using the BioArray HighYield RNA Transcript Labelling Kit T3 from Enzo Life Sciences (Farmingdale, NY). The final cDNA library construction and sequencing were performed at LC-Bio Technology Co, Ltd (Hang Zhou,China), using Illumina Hiseq 4000 platform.

Cell lines

The human gastric cancer cell lines BGC823 and SGC7901 were purchased from Fenghuibio (Changsha, China). Both cell lines were maintained in DMEM cell culture medium (Gibco, No. 11965-084) supplemented with 10% fetal bovine serum (FBS) (Gibco, No. 10082139), 100 IU/mL of penicillin, and 100 mg/mL of streptomycin (Genview, Carlsbad, CA) in a humidified 5% CO_2 atmosphere at 37°C.

q-PCR assay

The mRNA levels of PGAM1 in GC tissues and GC cell lines were evaluated by quantitative reverse transcription PCR (RT-qPCR) using the SYBR Green staining method using a Bio-Rad CFX 96 Touch Real-Time PCR Detection System (Bio-Rad, USA). β-Actin was used as an internal control. The relative change of PGAM1 gene was calculated according to the $2^{-\Delta\Delta Ct}$ method [17].

Primers specific for PGAM1 and internal reference gene are:

Gene	primers
homo-PGAM1-F1 :	GTGCAGAAGAGAGCGATCCG
homo-PGAM1-R1 :	CGGTTAGACCCCCATAGTGC
homo-ACTIN-F1	CATCCGCAAAGACCTGTACG
homo-ACTIN-R1	CCTGCTTGCTGATCCACATC

Cell infections and purification

The lentiviral vector pWSLV-sh09 (Supplementary figure 1) expressing a PGAM1-1-targeting shRNA were transfected into 293T cells using the Lipofectamine LTX reagent (Invitrogen). BGC823 and SGC7901 cells (2×10^5) were seeded into 12-well cell culture plates and cultured for 18 hours. Cells were then infected with 100 μL of virus-containing supernatant from transfected 293T cells and incubated for 48 hours. Infection with virus from the pWSLV empty vector was used as a negative control. Infected cells were purified by flow cytometry on the basis of green fluorescent protein (GFP) expression.

Cell proliferation assay

Analysis of cell growth/proliferation was performed by measurement of colorimetric conversion of the CCK-8 tetrazolium salt, an indicator of viable cells. For the assay, PGAM1 knockdown BGC823 and SGC7901 cells and negative controls were seeded in 96-well plate (2×10^5 each) in 200 μL culture media and cells were allowed to attach. At different time points (0h, 24h, 48h, 72h), 20 μL of CCK-8 reagent (Cell Counting Kit-8, Dojindo, Japan) was added to 5 wells of the plate and incubated for 2h at 37 °C. The optical density (OD) of each well was then recorded at 450 nm using a microplatereader (BioTekSynergy-4). The growth curves for PGAM1 knockdown and control cells were generated by plotting the average of the 5 wells for each time point.

Cell cycle and apoptosis assays

Cell cycle analysis was performed using propidium iodide (PI) staining. Cells were synchronized by incubation in starvation medium (containing 0.5% FBS) for 48 hours. Complete medium was then added to activate cell cycle entry and cells were cultured for 24h. BGC823 and SGC7901 cells with and without PGAM1 knockdown were harvested with 0.25% trypsin (Millipore, Shanghai, China) and re-suspended in 100 μL PBS. The cells were gently dripped into chilled 75 % ethanol and fixed at -20°C overnight. After washing 3 times with sterile PBS to remove residual ethanol, cells were treated with 20 μg/mL RNase-A at 37 °C for 10 min and then stained with 10 μg/mL PI for 10 min at room temperature. DNA content was measured by flow cytometry.

Apoptosis was measured using the Annexin-V/PI double staining method. BGC823 and SGC7901 cells were dissociated and washed and resuspended in sterile PBS. Cells were labeled with Annexin V-FITC and PI (AnnexinV-FITC Apoptosis Detection Kit, Beyotime Institute of Biotechnology, Haimen, China), according to manufacturer's instructions. The DNA content and apoptosis of GC cells were measured by flow cytometry (BD, Biosciences, California, USA). The flow cytometry data was analyzed by CellQuest (BD, Bioscience) and MultiCycle software.

Cell migration assay

BGC823 and SGC7901 cells were incubated in starvation medium (containing 0.5% FBS) overnight. Cells were then harvested and approximately 1×10^5 cells were added to a Transwell chamber (Millipore, Shanghai, China). The chambers were placed into wells of a 24-well plate containing complete (10% FBS) DMEM media and cultured in 5 % CO_2 incubator at 37 °C for 24 hours. Cells that did not migrate through the membrane were removed using a disinfected cotton swab. Cells that migrated through the membrane were stained with crystal violet and photographed under an inverted microscope. Stained cells from each group were counted in five defined areas of 200 μm^2 in the center of a random field of vision. Cells that migrated further into the well of the 24-well plate were detected by CCK-8 reagent and the OD values of the culture medium were recorded at 450 nm in a microplate reader.

Wound-healing assay

BGC823 or SGC7901 cells (1×10^6 each) with or without PGAM1 knockdown were seeded into wells of 12-well plate. After the cells reached 80% confluence, a disinfected 10-μL tip was used to make a vertical wound in each well. Cells were gently washed with sterile PBS to remove the cell fragments and continuously cultured in complete media. Wound closure was observed at different time points (0h, 24h, 48h, and 72h) and images were captured using an inverted microscope. ImageJ software was used to calculate the wound-healing rate according to the following equation :

Flow cytometry assay for migration-related proteins MMP2, MMP9 and ICAM-1

To analyze the expression of metastasis and migration-related proteins, cells (2×10^5 each) in the PGAM1 knockdown group and empty vector control group were harvested and washed with sterile PBS. For intracellular antigen detection, the cells were fixed by using eBioscience™ Fixation buffer (No. 00-5223-56, invirtogen) for 30 min, and then penetrated by diluted Permeabilization Buffer 10X (No. 00-8333-56, invirtogen) for another 20 min with the PE-conjugated primary antibody matrix metalloproteinases 2 (MMP2, No. ab51125, Abcam) or MMP9 (No. ab194314, Abcam) in it. For detecting cell surface antigens, cells were incubated with PE-conjugated primary antibody of intercellular cell adhesion molecule-1 (ICAM-1) (No. ab27582, Abcam) at room temperature for 10 min. Expression levels were measured by flow cytometry. Flow cytometry data was analyzed by CellQuest (BD, Bioscience).

Western blot analysis

For western blot analysis, BGC823 and SGC7901 cells (3×10^7), with or without a PGAM1 knockdown were washed with PBS and lysed in RIPA buffer (CWbiotech, Beijing, China) supplemented with protease inhibitors (CWbiotech, Beijing, China) on ice for 10 min. BCA protein assay (Beyotime Institute of Biotechnology, Haimen, China) was used to quantify protein in the lysates of each sample. Approximately 20 μg of each protein sample were separated in 12% Tris-glycine gels and transferred onto polyvinylidene fluoride (PVFD) membranes. Blots were blocked in 5% nonfat milk for 1 h, washed three times with TBST, and incubated with primary antibodies overnight at 4 °C in blocking buffer. Anti-GAPDH antibodies were used as a loading control. Blots were washed 3X with TBS, and incubated with horseradish peroxidase (HRP)-labeled secondary antibody at room temperature for 1h under gentle shaking. The blots were washed again with TBS and then developed with chemiluminescent substrate (EasySeeVR Western Blot Kit, TransGen Biotech, Beijing, China) for 1 min. Signals were detected by exposure of the blots to x-ray film. The list of antibodies is shown in table 2.

Immunohistochemistry

For PGAM1 IHC, thin sections from LNM tissue, CIS tissues and matched paracancerous tissues of GC patients were embedded in paraffin, deparaffinized by xylene and dehydrated by using graded alcohol solutions. The sections were incubated in 0.01 M citrate buffer (pH 6.0) to rehydrate at 121 °C for 2 min in a pressure vessel. Sections were incubated in 3% hydrogen peroxide at room temperature for 15 minutes to eliminate the activity of endogenous peroxidase, washed three times with PBS, blocked with PBS containing 5% BSA (No. p0007, Beyotime Institute of Biotechnology, Haimen, China) at room temperature

for 30 minutes and incubated with primary antibody at 4°C overnight. After washing with PBS, secondary antibody (UltraSensitive^{TM} SP (Mouse/Rabbit) IHC Kit, KIT-9710, Maixin, FuZhou, China) was added to samples and incubated at room temperature for 20 min, and the chromogenic reaction was activated with DAB (DAB-0031, Maixin, FuZhou, China). Hematoxylin was added as a counterstain. The expression of PGAM1 in samples was observed and photographed with an inverted microscope. Scoring was performed by two people in a double-blind reading, and compared to unstained sections as a negative control. The positive cells in five visual fields of each slice were counted and graded according to the following standard, unstained, zero points, negative; faint yellow, one points, weak positive; pale brown, two points, moderately positive; dark brown, three points, strong positive. The percentage of positive cells was graded as follows: <10%, zero points; 11%-25%, one points; 26%-50%, two points, 51%-75%, three points, >75%, four points. By multiplying positive cell score and percentage score, ≤ 6 defined as low expression, ≥6 defined as high expression.

The in vivo effect of PGAM1 in a murine GC xenograft model

Experimental mouse protocols were approved by the Ethics Committees of the First Hospital of Jilin University (License No. 2020-0455), and all experimental procedures conformed to IACUC policy. Immunodeficient NPSG (NOD-Prkdcscid IL2rgtm201(-/-)/V) mice (male, 6 weeks old) were obtained from Beijing GeneX Health Co. ltd and maintained in specific pathogen-free (SPF) conditions. Mice were randomly divided into four groups (n=6). Each cohort of mice received a subcutaneous injection in the flank with one of the four cell lines: BGC823 or SGC7901, control cells or with PGAM1 knockdown (5×10^6 cells per mouse in 0.1ml DMEM/Matrigel (1:1 v/v). All mice were fed under standardized animal house conditions (12 h light/dark cycle at 22 °C, and relative humidity 50%) with free access to food and water. The growth of tumors was measured every week using calipers. The tumor size was calculated according to the following formula: $V=1/2\times ab^2$ [maximum (a) and minimum (b) length of the tumor]. After approximately 6 weeks, mice were sacrificed, and the tumors were measured and weighed.

Data Analysis.

GraphPad Prism 7 software and spss 25.0 software were used to perform statistical analysis for all data. The results were analyzed using the Student' t test or Kruskal-Wallis test. Data were presented as the mean ± SD. Statistical significance was defined as $p < 0.05$.

Results

Aberrantly expressed mRNA in lymph node metastatic GC tissue

We initially performed total genome (mRNA) sequencing analysis of GC samples from three patients, comparing gene expression in cells from CIS, LNM, and paracancerous tissues. The sequencing results showed that 105 mRNAs were aberrantly expressed in LNM GC tissue compared to the CIS tissue (n=3).

Among them, 86 mRNAs were up-regulated and 19 mRNAs were down-regulated (figure 1A and B). The top ten significantly up-regulated mRNAs were HMGN3, MRPS26, CCND1, C12orf75, TPM1, CDK2AP1, ZNF292, PGAM1, STAU2, and GTF2IP4. The top three significantly down-regulated genes were NDUFA1, PARK7, and C14orf2 (figure 1A and B). The expression of PGAM1 in LNM tissues was markedly higher than in CIS tissues ($p < 0.01$).

PGAM1 was up-regulated in lymph node metastatic GC tissue and cell line.

The up-regulation of PGAM1 mRNA in LNM GC tissues was validated by q-PCR and protein levels were measured by IHC in tissues from an expanded cohort of 56 GC patients (figure 1C-H). q-PCR results showed that in LNM GC tissue, PGAM1 was up-regulated 3.05 ± 2.55-fold compared to CIS tissue (n=56) (figure 1C). Likewise, PGAM1 was upregulated in the metastatic SGC7901 cell line 1.96 ± 0.24 fold compared to non-metastatic BGC823 cells (n=5) (figure 2B). According to standard grading (figure 1D), IHC results showed that in CIS tissues, 6 cases were negative (10.7%), 29 cases were weakly positive (51.8%), 12 cases showed moderate expression levels (21.4%) and 9 cases (16.1%) were strongly positive for PGAM1. In LNM tissues, there were 3 negative cases (5.3%), 12 cases were weakly positive (21.4%), 15 cases were moderately positive (26.8%) and 26 cases were strongly positive (46.4%). By comparison, in paracancerous tissues 38 cases (67.9%) were negative, 14 cases (25%) were weakly positive, 4 cases (7.1%) were moderately positive; there were no strongly positive cases (figure 1E and F). By multiplying the positive cell score and percentage score, we generated a scale of the IHC data in which a score of ≤ 6 was defined as low expression and ≥ 6 was defined as high expression. Transforming the data in this manner, we found that in CIS tissues, 53 cases (94.6%) showed low expression of PGAM1, while only 3 cases (5.4%) expressed high levels of PGAM1. Critically, in LNM tissues, 18 cases (32%) displayed high PGAM1 expression and 38 cases (68%) showed low expression. In contrast to the tumor tissues, all 56 samples of paracancerous tissues displayed low PGAM1 levels, (figures 1G and H).

In order to assess the potential role of PGAM1 in clinical outcomes, we performed a follow-up analysis of GC patients to determine whether PGAM1 expression correlated with disease recurrence or death. We found that two years after surgery, tumor free survival was observed in 32 patients, 14 patients died, 8 patients had disease recurrence, and 2 patients could not be contacted (no data). The correlation of PGAM1 expression levels in CIS and LNM tissues with prognosis is shown in figures 1I and 1J. There was no significant difference in PGAM1 expression in CIS tissue between dead/recurrent patients and survivors (p=0.308). However, in LNM tissues of patients, PGAM1 expression levels in dead/recurrent patients were significantly higher than the expression levels in survivors (p=0.02), which indicates that PGAM1 levels in LNM GC tissue is an independent risk factor of poor prognosis. These findings support the hypothesis that PGAM1 is a pathogenic factor in lethal metastatic GC. In order to further explore the role of PGAM1 in GC, we developed a system using two GC cells lines with differential metastatic behavior, and manipulated PGAM1 expression in *in vitro* and *in vivo* correlates of human gastric cancer.

Knockdown of PGAM1 in GC cells

We transduced SGC7901 (metastatic) and BGC823 (non-metastatic) GC cell lines with lentivirus particles expressing a PGAM1 shRNA targeting construct (pWSLV-sh-09-PGAM1), and purified infected cells by flow cytometry on the basis of GFP expression. Fluorescent imaging confirmed that the purified cell lines were both over 95% GFP positive (figures 2A and B). Empty vector controls were infected at the same efficiency (data not shown). The expression levels of PGAM1 in the two GC cell lines were measured by q-PCR. PGAM1 mRNA levels in the knockdown GC cell lines were reduced to 22.72% ± 2.6% in BGC823 cells and 11.14% ± 1.74% in SGC7901 cells compared to cells expressing an empty vector control (figures 2C and D).

Depletion of PGAM1 inhibited cell proliferation of GC cell lines

Cell growth in PGAM1 knockdown and control cell lines was determined by measuring the increase in viable cells over a 72 hour time course using the CCK-8 tetrazolium salt. We found PGAM1 knockdown in both BGC823 and SGC7901 cell lines impaired proliferation after 48 and 72h of culture relative to control cells expressing empty vector (figures 2E and F). PGAM1 knockdown in BGC823 inhibited proliferation by 30% after 48 hours (OD_{450} 1.23± 0.09 versus 1.75± 0.11) and 31.06% after 72 hours (OD_{450} 1.62± 0.24 versus 2.35± 0.12). Likewise, PGAM1 knockdown blunted the proliferation of SGC7901 by 30.2% after 48 hours (OD_{450} 1.83± 0.16 versus 2.62± 0.17) and 32.1% after 72 hours (OD_{450} 2.08± 0.18 versus 3.06± 0.20).

PGAM1 knockdown affects cell cycle progression of GC cells.

To determine the cell cycle distribution and kinetics of both GC cell lines, cells were serum starved in DMEM with 0.5% FBS and then incubated for 24 hours in complete medium to activate cell cycle entry. DNA content was measured by flow cytometry using propidium iodide staining. As shown in figures 2G-J, the cell cycle distribution of control BGC823 cells was as follows: 40.19 ± 7.8% in G_0/G_1 and 52.59 ± 9.4% in S phase. In contrast, BGC823 with PGAM1 knockdown showed 55.18 ± 7.5% in G_0/G_1 and 41.72 ± 6.8% in S phase. Likewise, in control SGC7901 cells, 61.49 ± 7.7% of the population was in G_0/G_1 while 34.71% ± 6.1% were in S phase. PGAM1 knockdown in SGC7901 resulted in 79.85% ± 6.3% in G_0/G_1 and 17.68% ± 7.1% in S phase. These data indicate that loss of PGAM1 impairs cell cycle progression and results accumulation of cells in $G_0/G_{1,}$ while reducing the percentage of cells in S phase, suggesting that PGAM1 promotes cell proliferation in GC.

PGAM1 knockdown did not affect apoptosis of GC cells.

We next assessed the role of PGAM1 in the regulation of apoptosis in asynchronously growing cells. Annexin-V/ PI staining showed that depletion of PGAM1 did not affect apoptosis of either GC cell line. Combined early and late stage apoptosis of BGC823 cells represented 18.19% and 15.81% of the total population in control and knockdown cells, respectively. Likewise, apoptosis of SGC7901 was found to be 5.61% in the parental cells and 9.5% in the PGAM1 knock-down (figure 3A and C). Statistical analysis confirmed that the differences in apoptosis between the parental and PGAM1 knock-down derivatives of

either cell line were not significant (figure 3B and D). These findings indicate that PGAM1 does not play a critical role in regulating apoptosis in GC.

PGAM1 knockdown inhibited migration of GC cells

We next examined the potential involvement of PGAM1 in GC cell migration in transwell and wound healing assays as an *in vitro* correlate of metastasis. Figure 4A-C shows that depletion of PGAM1 impaired migration of both BGC823 and SGC7901. Wound repair rates were significantly decreased in PGAM1 knockdown compared to parental cells in both BGC823 (3.4% versus 27.2% wound closure) and SGC7901 (11.3% versus 34.4% wound closure) at the 24h time point. The differences in wound recovery rates between control and knockdown GC cells were significant throughout the course of the experiment.

Likewise, in a 24 hour transwell migration assay (figure 4D-H), PGAM1 knockdown decreased the number of cells migrating through a microporous barrier in both cell lines relative to control cells (BGC823: 51±7 versus 81±13 cell per field, 37% inhibition; SGC7901: 83±11 versus 143±14 cells per field, 41.9% inhibition)(figures 4E and F). Similarly, analysis of cells that migrated further into the lower chamber showed the same pattern. The number of cells in the lower chamber was reduced in knockdown cells relative to controls (figure 4G and H). These results indicate that PGAM1 plays a role in promoting migration of GC cells.

PGAM1 knockdown inhibited the expression of migration-related proteins.

We next analyzed the effect of PGAM1 knockdown on the expression of proteins involved in migration and metastasis of GC. Flow cytometric analysis showed that BGC823 and SGC7901 cells with a PGAM1 knockdown displayed impaired expression of migration-related proteins (ICAM-1, MMP2, and MMP9) relative to control cells (figure 5A-D). These findings suggest that PGAM1 may drive GC metastasis by upregulating proteins that degrade the extracellular matrix and enhance cell adhesion and migration.

PGAM1 knockdown decreased the phosphorylation of Src, FAK, and Paxillin

In order to further explore this possibility, we measured the expression and activation of migration-related signaling proteins including the Src and FAK kinases as well as the focal adhesion protein Paxillin in GC cells by western blot. We found that phosphorylated forms of Src, FAK, and Paxillin were markedly decreased in both BCG823 (figure 5E) and SGC7901 (figure 5F) PGAM1 knockdown cells relative to controls, with no effect on total protein levels, indicating that PGAM1 may regulate cytoskeletal signaling in GC. Western analysis also confirmed the marked repression of PGAM1 protein expression in the knockdown cells. This result suggests that PGAM-1-mediated activation of the Src/FAK/Paxillin pathway may play a role in metastasis of gastric cancer.

PGAM1 knockdown inhibited GC cell growth in vivo

The *in vivo* growth kinetics of subcutaneous PGAM1-deficient tumors were assayed in immunodeficient NPSG mice. As shown in figure 6A and B, PGAM1 depletion decreased the growth rate of both cell lines in

mice compared to control cells, resulting in reduced tumor bulk and weight after 6 weeks of *in vivo* growth. As shown in figure 6C, PGAM1 knockdown resulted in reduced tumor volume relative to control tumors throughout the course of the experiment. Body weight measurements indicated that the body weights of mice injected with control cells decreased more rapidly than mice with PGAM1-deficient tumors, indicating that PGAM1 increases the pathogenicity of disease (figure 6D). Collectively, these results suggest that targeting PGAM1 inhibits the growth and aggressiveness of gastric cancer *in vivo*.

Discussion

Compared to normal tissues, the metabolic rate, particularly the glycolytic rate of cancer cells is significantly increased due to mitochondrial dysfunction. Phosphoglycerate mutase 1 (PGAM1) is one of the key glycolytic enzymes in the cytoplasm that regulates this process. During glycolysis, PGAM1 converts 3-phosphoglycerate (3-PG) to 2-phosphoglycerate (2-PG) to release energy and plays a role in cancer carcinogenesis [18]. This enzyme is up-regulated in a variety of human cancers, including those of the lung [19], breast [18], prostate [20], bladder [11], liver [8], kidney [12], colon [7], brain [21] and head and neck [14]. Further, clinical studies have shown that overexpression of PGAM1 was associated with poor prognosis of patients with lung adenocarcinoma [19], hepatocellular carcinoma [8] and oral squamous cell carcinoma [14]. However, the role of PGAM1 in gastric cancer, a metastatic disease with a poor prognosis, is still unknown.

In the present study, LNM GC tissue and paired CIS tissue were collected from 3 GC patients using laser capture microdissection, which minimizes interference from non-specific tissue and increases the accuracy of mRNA and protein detection. Results of high throughput mRNA sequencing showed that PGAM1 was significantly up-regulated in lymph node metastatic GC tissue compared to the CIS tissue, which indicated PGAM1 may play a critical role in GC metastasis.

Previous studies have shown that PGAM1 regulates diverse aspects of tumor biology. For instance, studies from Evans *et al* and Engel *et al*. showed that the PGAM inhibitor MJE3 attenuated PGAM1 expression and inhibited proliferation of breast cancer cells [18, 22]. Likewise, down-regulation of PGAM1 significantly inhibited cell growth of hepatocellular carcinoma [8]. In addition, Hitosugi *et al*. reported that PGAM1 expression was positively correlated with tumor size, likely due to its ability to coordinate glycolysis and biosynthesis to promote cell proliferation and tumor growth [15]. In this study, we have shown that PGAM1 can play a novel role in the growth and proliferation of GC as well. Stable knockdown of PGAM inhibited the proliferation of GC cell lines representative of both metastatic (SGC7901-derived from lymph node metastatsis) and non-metastatic (BGC823-derived from gastric adenocarcinoma tissue) disease *in vitro.* Importantly, we found that PGAM1 knockdown inhibited the growth of metastatic SGC7901 to a greater extent than BGC823 cells. The same trend was observed in a murine *in vivo* xenograft model of GC as well: reduction of tumor volume by PGAM1 knockdown was more pronounced in SGC7901 compared to the non-metastatic BGC823 cell line suggesting the PGAM1 plays an important role in GC metastasis. We have also explored possible molecular mechanisms driving PGAM1-dependent tumor cell growth and survival. Cell cycle analysis showed that PGAM1 knockdown induced an

accumulation of cells G0/G1 and a reduction of cells in S phase in BGC823 and SGC7901, which may be explained by reduction in PGAM1-dependent energy production. Compared to normal tissues, tumor tissues accumulate more glucose which could be used as a molecular source for anabolic biosynthesis of macromolecules involved in tumor cell proliferation [23]. Consequently, depletion of PGAM1 may inhibit glycoysis, impairing tumor cell energy production and impairing tumor growth. Our findings are in agreement with previous studies showing that other genes involved in glycolysis were up-regulated in several types of cancers [24]. Thus, PGAM1 and other glycolysis-related proteins such as HK, PFK-1 and HIF-1α, may be potential candidates for therapeutic targeting in cancer therapy.

PGAM1 has also been shown to regulate apoptosis in tumor cells. Xu *et al*. reported that knockdown of PGAM1 expression induced glioma cell apoptosis by upregulating Bax expression, downregulating Bcl-2 expression, and activating the caspase-3 signal in glioma cells [21]. However, in our study, we observed no significant change in the apoptotic rate in GC cell lines after PGAM1 depletion, suggesting that PGAM1 may have distinct functions in tumors derived from different tissues.

Interestingly, it has been shown that some metabolic enzymes have functions in tumor physiology that are independent of their enzymatic activities [25–27]. Zhang *et al* reported that PGAM1 knockdown decreased metastatic potential of breast cancer cells, demonstrating that PGAM1 can promote cancer cell migration in a manner that was independent of its metabolic activity. Furthermore, α-smooth muscle actin (ACTA2) was identified as a PGAM1-associated protein, and PGAM1 modulated actin filament assembly, cancer cell motility, and migration via a direct interaction with ACTA2 [16]. These results suggest that PGAM1 plays a role in tumor cell migration and actin cytoskeleton reorganization. In a related study, Xu et al. found that the migration and invasion of glioma cells were significantly reduced by siRNA targeting of PGAM1, which was related to repressed MMP2 and MMP9 protein expression [28]. These data are in agreement with our findings which implicate a role for PGAM1 in multiple steps of the metastatic process in GC through upregulation of MMP2, MMP9 and ICAM-I. The metalloproteinases MMP2 and MMP9 are critical for tumor invasion, angiogenesis, metastasis and recurrence via degradation of the extracellular matrix [29] whereas ICAM-I promotes cell adhesion and migration to metastatic sites [30]. These findings raise the possibility that PGAM1 may have non-catalytic functions in GC, particularly in light of our findings that PGAM1 expression levels are highest in GC metatatic tissues and cell lines.

To explore in greater molecular detail the role of PGAM-1 in metastasis, we analyzed the effects of PGAM1 on metastasis-related signaling pathways. The complex process of cell migration requires precise cooperation of many proteins and signaling pathways that drive cellular movement [31]. Among metastasis-related proteins, the intracellular tyrosine kinase FAK is a central mediator of integrin signaling and an important component of other signaling triggered by cell surface receptors which contributes to the pathogenesis of cancer [32]. By recruiting c-Src, activated FAK forms a FAK-Src signaling complex that mediates the phosphorylation of paxillin, which is a scaffolding molecule [33] and adapter protein capable of activating diverse signaling pathways that regulate cell migration [34, 35]. The FAK/Src/paxillin pathway modulates the rate of adhesion formation and disassembly, which controls the

migration of cells [36]. According to our western blot analysis, PGAM1 depletion impaired the phosphorylation and activation of FAK, Src and paxillin, suggesting that PGAM1 plays a role in migration, invasion and metastasis of GC cells via activation of the FAK/Src/paxillin signaling axis.

To establish a link between PGAM1 and clinical outcomes in patients, we analyzed PGAM1 expression levels in CIS tissues and LNM tissues in an expanded cohort of GC patients by q-PCR and IHC assays. Our results verified that there was high expression of PGAM1 in LNM tissues compared with CIS tissues in 56 cases of GC patients. The outcomes for the 56 patients were investigated in a two year follow-up study. Among them, 32 cases showed tumor free survival, 14 patients died, 8 patients experienced disease recurrence, and 2 cases could not be contacted (loss of data). It was shown that the high expression of PGAM1 in LNM tissue rather than its expression in CIS is an independent risk factor indicating poor prognosis in GC, suggesting that PGAM1 or its downstream effectors may be potential therapeutic targets.

In summary, we have shown that PGAM1 was preferentially up-regulated in LNM GC tissue and a LNM tissue-derived cell line compared to non-metastatic counterparts. Knocking down PGAM1 expression in two GC cell lines, BGC823 (non-metastatic) and SGC7901 (metastatic) inhibited cell proliferation *in vitro* and *in vivo*, induced G0/G1 cell cycle accumulation, and impaired cell migration. Further mechanistic analysis showed that knocking down PGAM1 impaired the expression of metalloproteinases MMP2 and MMP9, as well as the adhesion molecule ICAM-1, and inhibited cytoskeletal activation by blocking FAK/Src/paxillin signal transduction, suggesting a possible molecular mechanism for PGAM1-mediated enhancement of migration and metastasis. In light of previous data showing a physical association between PGAM-1 and the actin cytoskeleton in breast cancer, our data suggest that PGAM-1 may regulate metastatic behavior in GC through a mechanism that is independent of its catalytic activity.

Finally, we have shown that high expression of PGAM1 in LNM tissue correlates with disease recurrence and mortality in GC patients, suggesting that PGAM1 may be an important biomarker and driver of aggressive, metastatic GC. Our studies indicate that biological targeting of PGAM1 or PGAM1-dependent signaling pathways may inhibit GC growth and metastasis and improve the prognosis of GC patients.

Abbreviations

α-smooth muscle actin, ACTA2;

carcinoma in situ, CIS;

gastric cancer, GC;

green fluorescent protein, GFP;

horseradish peroxidase, HRP;

immunohistochemistry, IHC;

institutional animal care and use committee, IACUC;

intercellular cell adhesion molecule-1, ICAM-1;

lymph node metastasis, LNM;

matrix metalloproteinases 2,mmp2;

matrix metalloproteinases 9,mmp9;

optical density, OD;

polyvinylidene fluoride, PVFD;

propidium iodide, PI;

quantitative PCR, q-PCR;

specific pathogen-free, SPF;

upregulation of phosphoglyceric acid mutase, PGAM;

3-phosphoglycerate, 3-PG;

2-phosphoglycerate, 2-PG;

Declarations

Acknowledgments:

None

Funding:

This project was funded by the First Hospital of Jilin University

Author's contributions:

Helei Wang performed the main experiments and wrote the paper. Jian Suo and Nicholas A. Cacalano conceived and designed the experiments. Daguang Wang performed the RT-qPCR assay and data analysis. Zitian Wang cultured all cells used in this experiment. Lei Wang performed the flow cytometry test. Zhicheng Liu performed the WB test.

Statements and Declarations

Competing Interests:

All authors declare no competing interests.

Ethics Approval and Consent to Participate:

All ethics approvals are provided in our Supplementary Data file, which includes approvals for animal work. No individual data is presented. All clinical information has been de-identified.

Availability of Data:

All data sets will be made available upon request.

References

1. Bray F, Ferlay J, Soerjomataram I, Siegel RL, Torre LA, Jemal A: **Global cancer statistics 2018: GLOBOCAN estimates of incidence and mortality worldwide for 36 cancers in 185 countries.** CA Cancer J. Clin. **68,** 394-424 (2018)
2. Chen WQ, Li H, Sun KX, Zheng RS, Zhang SW, Zeng HM, Zou XN, Gu XY, He J: **[Report of Cancer Incidence and Mortality in China, 2014].** Zhonghua Zhong Liu Za Zhi**. 40,** 5-13 (2018)
3. Ohashi T, Komatsu S, Ichikawa D, Miyamae M, Okajima W, Imamura T, Kiuchi J, Kosuga T, Konishi H, Shiozaki A, et al: **Overexpression of PBK/TOPK relates to tumour malignant potential and poor outcome of gastric carcinoma.** Br. J. Cancer **116,** 218-226 (2017)
4. Duo-Ji MM, Ci-Ren BS, Long ZW, Zhang XH, Luo DL: **Short-term efficacy of different chemotherapy regimens in the treatment of advanced gastric cancer: a network meta-analysis.** Oncotarget **8,** 37896-37911 (2017)
5. Cervantes A, Roda D, Tarazona N, Rosello S, Perez-Fidalgo JA: **Current questions for the treatment of advanced gastric cancer.** Cancer Treat. Rev. **39,** 60-67 (2013)
6. Fothergill-Gilmore LA, Watson HC: **The phosphoglycerate mutases.** Adv. Enzymol. Relat. Areas Mol. Biol. **62,** 227-313 (1989)
7. Liu L, Wang S, Zhang Q, Ding Y: **Identification of potential genes/proteins regulated by Tiam1 in colorectal cancer by microarray analysis and proteome analysis.** Cell. Biol. Int. **32,** 1215-1222 (2008)
8. Ren F, Wu H, Lei Y, Zhang H, Liu R, Zhao Y, Chen X, Zeng D, Tong A, Chen L, et al: **Quantitative proteomics identification of phosphoglycerate mutase 1 as a novel therapeutic target in hepatocellular carcinoma.** Mol. Cancer **9,** 81 (2010)
9. Turhani D, Krapfenbauer K, Thurnher D, Langen H, Fountoulakis M: **Identification of differentially expressed, tumor-associated proteins in oral squamous cell carcinoma by proteomic analysis.** Electrophoresis **27,** 1417-1423 (2006)
10. Huang LJ, Chen SX, Luo WJ, Jiang HH, Zhang PF, Yi H: **Proteomic analysis of secreted proteins of non-small cell lung cancer.** Ai Zheng **25,** 1361-1367 (2006)
11. Peng XC, Gong FM, Chen Y, Qiu M, Cheng K, Tang J, Ge J, Chen N, Zeng H, Liu JY: **Proteomics identification of PGAM1 as a potential therapeutic target for urothelial bladder cancer.** J. Proteomics

132, 85-92 (2016)

12. Li C, Shu F, Lei B, Lv D, Zhang S, Mao X: **Expression of PGAM1 in renal clear cell carcinoma and its clinical significance.** Int. J. Clin. Exp. Pathol. **8,** 9410-9415 (2015)
13. Liu ZG, Ding J, Du C, Xu N, Wang EL, Li JY, Wang YY, Yu JM: **Phosphoglycerate mutase 1 is highly expressed in C6 glioma cells and human astrocytoma.** Oncol. Lett. **15,** 8935-8940 (2018)
14. Zhang D, Wu H, Zhang X, Ding X, Huang M, Geng M, Li H, Xie Z: **Phosphoglycerate Mutase 1 Predicts the Poor Prognosis of Oral Squamous Cell Carcinoma and is Associated with Cell Migration.** J. Cancer **8,** 1943-1951 (2017)
15. Hitosugi T, Zhou L, Elf S, Fan J, Kang HB, Seo JH, Shan C, Dai Q, Zhang L, Xie J, et al: **Phosphoglycerate mutase 1 coordinates glycolysis and biosynthesis to promote tumor growth.** Cancer Cell **22,** 585-600 (2012)
16. Zhang D, Jin N, Sun W, Li X, Liu B, Xie Z, Qu J, Xu J, Yang X, Su Y, et al: **Phosphoglycerate mutase 1 promotes cancer cell migration independent of its metabolic activity.** Oncogene **36,** 2900-2909 (2017)
17. Livak KJ, Schmittgen TD: **Analysis of relative gene expression data using real-time quantitative PCR and the 2(-Delta Delta C(T)) Method.** Methods **25,** 402-408 (2001)
18. Evans MJ, Saghatelian A, Sorensen EJ, Cravatt BF: **Target discovery in small-molecule cell-based screens by in situ proteome reactivity profiling.** Nat. Biotechnol. **23,** 1303-1307 (2005)
19. Chen G, Gharib TG, Wang H, Huang CC, Kuick R, Thomas DG, Shedden KA, Misek DE, Taylor JM, Giordano TJ, et al: **Protein profiles associated with survival in lung adenocarcinoma.** Proc. Natl. Acad. Sci. U. S. A. **100,** 13537-13542 (2003)
20. Narayanan NK, Narayanan BA, Nixon DW: **Resveratrol-induced cell growth inhibition and apoptosis is associated with modulation of phosphoglycerate mutase B in human prostate cancer cells: two-dimensional sodium dodecyl sulfate-polyacrylamide gel electrophoresis and mass spectrometry evaluation.** Cancer Detect. Prev. **28,** 443-452 (2004)
21. Xu Z, Gong J, Wang C, Wang Y, Song Y, Xu W, Liu Z, Liu Y: **The diagnostic value and functional roles of phosphoglycerate mutase 1 in glioma.** Oncol. Rep. **36,** 2236-2244 (2016)
22. Engel M, Mazurek S, Eigenbrodt E, Welter C: **Phosphoglycerate mutase-derived polypeptide inhibits glycolytic flux and induces cell growth arrest in tumor cell lines.** J. Biol. Chem. **279,** 35803-35812 (2004)
23. Kroemer G, Pouyssegur J: **Tumor cell metabolism: cancer's Achilles' heel.** Cancer Cell **13,** 472-482 (2008)
24. Moreno-Sanchez R, Rodriguez-Enriquez S, Marin-Hernandez A, Saavedra E: **Energy metabolism in tumor cells.** FEBS J. **274,** 1393-1418 (2007)
25. Jiang Y, Li X, Yang W, Hawke DH, Zheng Y, Xia Y, Aldape K, Wei C, Guo F, Chen Y, Lu Z: **PKM2 regulates chromosome segregation and mitosis progression of tumor cells.** Mol. Cell. **53,** 75-87 (2014)

26. Luo W, Hu H, Chang R, Zhong J, Knabel M, O'Meally R, Cole RN, Pandey A, Semenza GL: **Pyruvate kinase M2 is a PHD3-stimulated coactivator for hypoxia-inducible factor 1.** Cell **145,** 732-744 (2011)
27. Yang W, Xia Y, Ji H, Zheng Y, Liang J, Huang W, Gao X, Aldape K, Lu Z: **Nuclear PKM2 regulates beta-catenin transactivation upon EGFR activation.** Nature **480,** 118-122 (2011)
28. Murray RH, Erler DV, Eyre BD: **Nitrous oxide fluxes in estuarine environments: response to global change.** Glob. Chang. Biol. **21,** 3219-3245 (2015)
29. Grzelczyk WL, Szemraj J, Jozefowicz-Korczynska M: **The matrix metalloproteinase in larynx cancer.** Postepy. Hig. Med. Dosw. (Online) **70,** 1190-1197 (2016)
30. Hubbard AK, Rothlein R: **Intercellular adhesion molecule-1 (ICAM-1) expression and cell signaling cascades.** Free Radic. Biol. Med. **28,** 1379-1386 (2000)
31. Vicente-Manzanares M, Horwitz AR: **Cell migration: an overview.** Methods Mol. Biol. **769,** 1-24 (2011)
32. McLean GW, Carragher NO, Avizienyte E, Evans J, Brunton VG, Frame MC: **The role of focal-adhesion kinase in cancer - a new therapeutic opportunity.** Nat. Rev. Cancer **5,** 505-515 (2005)
33. Bellis SL, Miller JT, Turner CE: **Characterization of tyrosine phosphorylation of paxillin in vitro by focal adhesion kinase.** J. Biol. Chem. **270,** 17437-17441 (1995)
34. Parsons JT: **Focal adhesion kinase: the first ten years.** J. Cell. Sci. **116,** 1409-1416 (2003)
35. Schlaepfer DD, Mitra SK: **Multiple connections link FAK to cell motility and invasion.** Curr. Opin. Genet. Dev. **14,** 92-101 (2004)
36. Webb DJ, Donais K, Whitmore LA, Thomas SM, Turner CE, Parsons JT, Horwitz AF: **FAK-Src signalling through paxillin, ERK and MLCK regulates adhesion disassembly.** Nat. Cell. Biol. **6,** 154-161 (2004)

Tables

Table 1 Information of patients in sequencing group

Sample No.	Gender	Age	Histological type	TNM classification	Clinical stage
1	Male	45	Moderately-low differentiated adenocarcinoma	T3N3a	IIIB
2	Male	68	Moderately-low differentiated adenocarcinoma	T3N3b	IIIB
3	Female	46	Moderately differentiated adenocarcinoma	T3N2	IIIA

Table 2 Antibodies information

Antibody	No.	Company	Dilution ratio
Anti-PGAM1	ab96622	Abcam	1:5000
GAPHD	ab181602	Abcam	1:5000
Anti-Src	ab47405	Abcam	1:2000
Anti-Scr (pY418)	ab40660	Abcam	1:1000
Anti-FAK	ab40794	Abcam	1:2000
Anti-FAK (pY397)	ab81298	Abcam	1:1000
Anti-Paxillin	ab32084	Abcam	1:2000
Anti-Paxillin (pY31)	ab4832	Abcam	1:1000
Goat anti-rabbit IgG (HRP)	ab6721	Abcam	1:10000

Figures

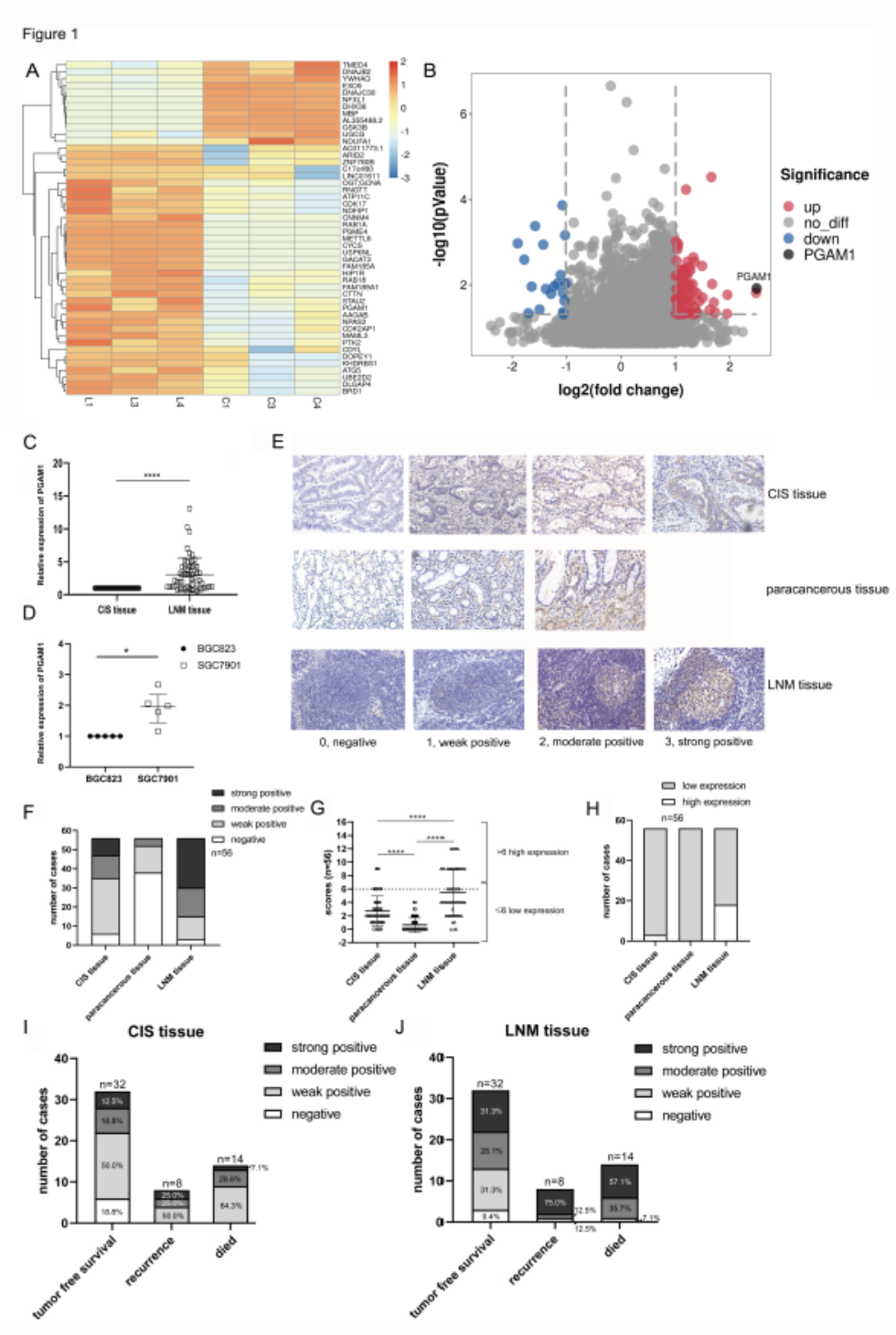

Figure 1

Elevated expression of PGAM1 mRNA and protein in GC lymph node metastases.

Panel A: Heatmap of cluster analysis of differentially expressed mRNAs (DEMs) in three GC patients. Red color indicates highly expressed DEMs and blue color indicates reduced expression. Panel B: Volcano plot of DEMs. The blue dots on the left side of the figure indicate down-regulated genes and the red dots

on the right side indicate up-regulated genes. (note: L: lymph node metastasis tissues; C: carcinoma *in situ* tissues). PGAM1 was one of the genes upregulated in GC lymph node metastases relative to CIS tissues. Panel C: mRNA expression of PGAM1 was elevated in LNM compared to CIS tissues from GC patients (n=56). mRNA expression levels were normalized to CIS tissues. Panel D: IHC grading standards used for analysis of PGAM1 protein expression in tissue sections. Panel E: Expression of PGAM1 mRNA is higher in a metastatic GC cell line (SGC7901) compared to a non-metastatic GC cell line (BGC823) (n=5). mRNA levels are normalized to BGC823. Panel F: Histograms show the distribution of IHC data in C among the four expression categories. Panel G: IHC data was transformed into high and low expression categories, as described in the text. Panel H: Histograms show quantitation of data in Panel E for CIS, LMN, and paracancerous tissues. Panels I and J: Correlation of PGAM1 IHC protein expression data in CIS and LNM tissues with clinical outcomes. Patient recurrence and death correlated with high PGAM1 expression in LNM tissues (panel H; p=0.02) but not CIS tissues (panel G; p=0.308). Statistical significance was determined using rank sum test. *p<0.05, ****p<0.0001.

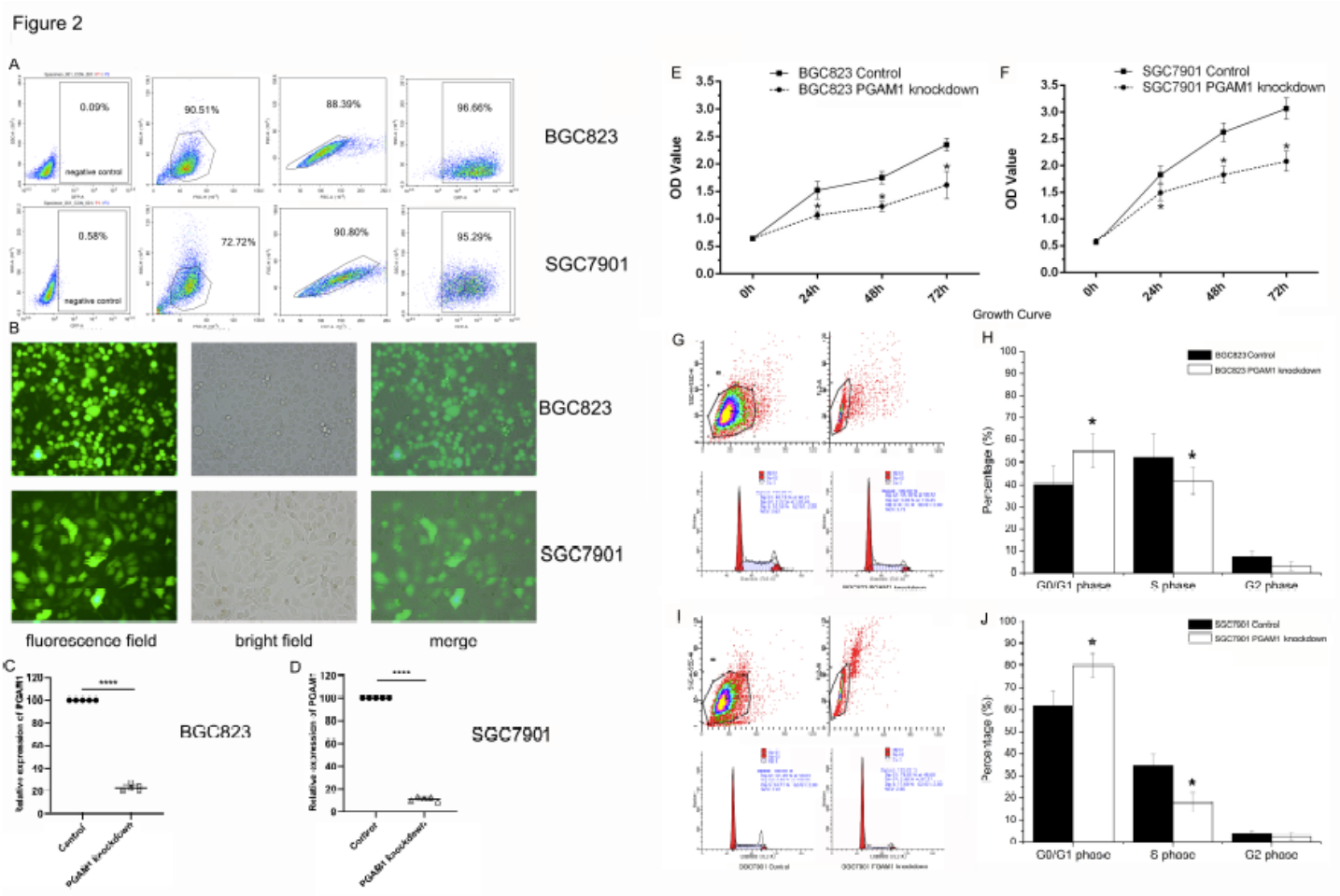

Figure 2

Effect of PGAM1 knockdown on *in vitro* growth and cell cycle progression of GC cells.

Panel A: Dot plots of flow cytometry data following sorting of GFP^+ cells. The plots show viable cells (left), single cells (middle), and GFP^+ cells (right). Panel B: Fluorescent microscopy of infected, sorted

cells. Green color indicates infected GFP^+ cells; both GC cell lines were over 95% GFP positive. Panel C and D: q-PCR analysis of PGAM1 knockdown in GC cell lines BCG823 and SGC7901. PGAM1 levels were normalized to negative control cells without PGAM1 knockdown. (n = 5) The data represent the mean ± SD of five independent experiments. One-way ANOVA and LSD test, ****$p < 0.0001$. Panels E and F: Growth curves of BGC823 and SGC7901, with or without PGAM1 knockdown, measured by CCK-8 assay. DNA content of BGC823 cells (panels G and H) and SGC7901 (panels I and J) was assessed by analysis of PI uptake. The bar graphs show the proportion of cells in each stage of the cell cycle The data represented the mean ± SD from three independent experiments. One-way ANOVA and LSD test, *: $p < 0.05$ compared with the negative control (n = 3).

Figure 3

Effects of PGAM1 knockdown on apoptosis and necrosis of GC cells.

Apoptosis of BGC823 (panels A and B) or SGC7901 (panels C and D) cells was assessed by Annexin V/PI double staining method. The bar graphs show the proportion of viable and apoptotic/necrotic cells. Viable cells were defined as Annexin V^-/PI^-, early apoptotic cells as Annexin V^+/PI^-, and late apoptotic/necrotic cells as Annexin V^+/PI^+. The data represent the mean ± SD from three independent experiments. One-way ANOVA and LSD test, *: $p < 0.05$ compared with the control (n = 3).

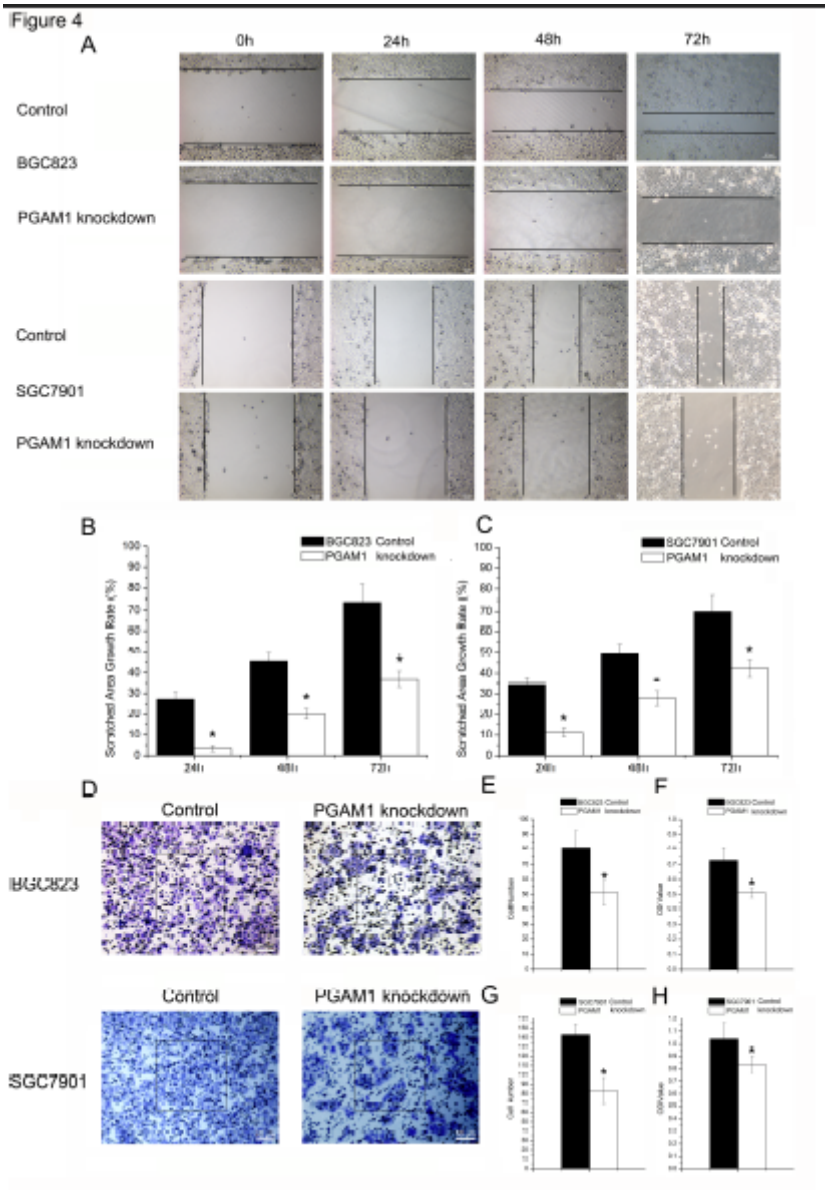

Figure 4

PGAM1 knockdown inhibits migration of GC cells

Wound-healing assay of BGC823 (panel A, Top) and SGC7901 (panel A, Bottom), with or without PGAM1 knockdown over a 72 hour time course. Quantitation of the scratched area growth rate for BGC823 (panel B) and SGC7901 (panel C) was calculated according to the formula: scratched area growth rate = ((wound area$_{(0h)}$ - wound area $_{(\text{each time point})}$)/ wound area$_{(0h)}$))×100%). The data represent the mean ± SD from three independent experiments. One-way ANOVA and LSD test, *: $p < 0.05$ compared to control (n = 3). Panel D: Transwell migration assay of BGC823 (Top) and SGC7901 (Bottom), with and without PGAM1 knockdown. Cells that migrated through the membranes of the transwell chambers were stained with crystal violet and counted. The square (200 μm^2) in the center of each field of vision shows the area used for cell counts. Panels E and F: Quantiation data in panel D. Panels G and H: Cells that migrated through the membrane and into the lower chamber were stained with the CCK-8 reagent. Shown are the

OD_{450} values reflecting relative cell numbers. The data represented the mean ± SD from three independent experiments. One-way ANOVA and LSD test, *: $p < 0.05$ compared with control (n = 3).

Figure 5

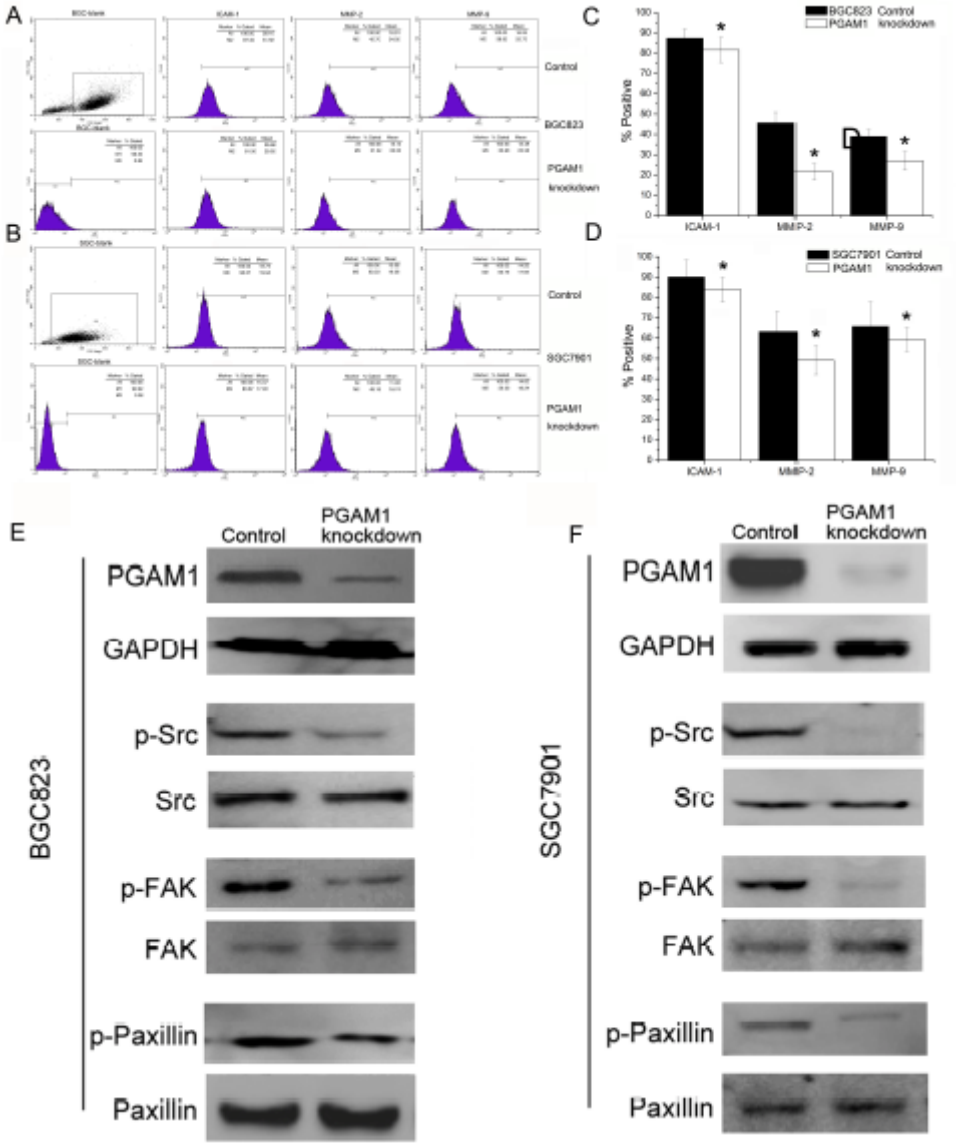

Figure 5

PGAM1 knockdown reduces the expression of adhesion and metastatic factors and impairs cytoskeletal signaling.

Cell surface expression of ICAM-1, MMP-2, and MMP-9 in BGC823 (panel A) and SGC7901 (panel B), measured by flow cytometry. Panels C and D: Quantitation of data shown in A and B, as per cent positive cells in the population for each marker. The data represent the mean ± SD from three independent experiments. One-way ANOVA and LSD test, *: $p < 0.05$ compared with control (n = 3). Panels E and F: Approximately $1X10^7$ BCG823 or SGC7901, with or without PGAM1 knockdown were lysed and protein extracts were analyzed by Western blot for PGAM1 protein levels and phosphorylated Src, FAK, and paxillin. Blots for total protein for each sample and GAPDH are shown as loading controls.

Figure 6

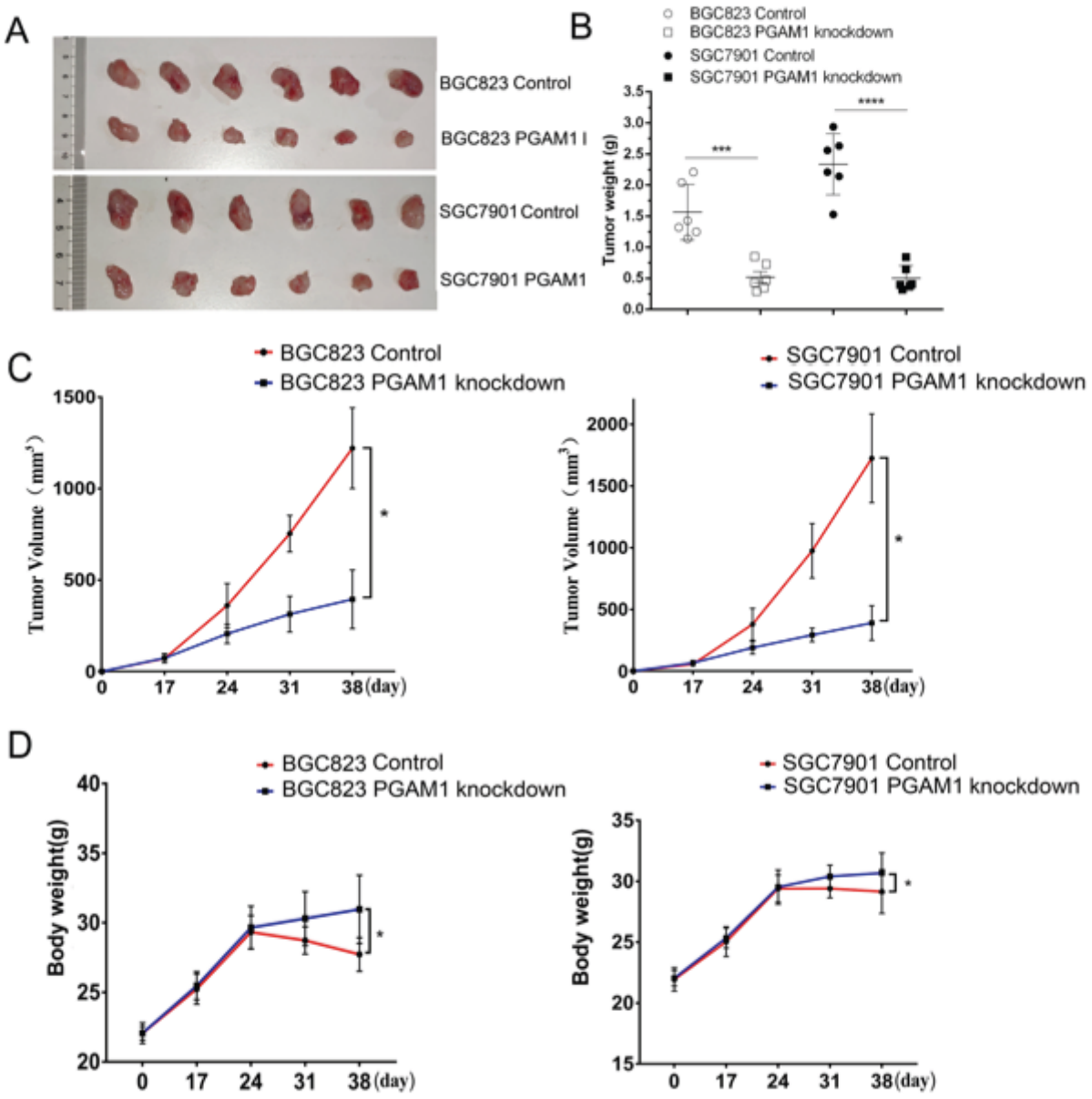

Figure 6

PGAM1 knockdown inhibits the growth of subcutaneous GC tumors in immunodeficient mice.

Approximately 1X10^6 BGC823 or SGC7901 cells, with or without PGAM1 knockdown were injected into the flank of NPSG mice and tumor size was measured with calipers. After six weeks, mice were sacrificed and tumors were weighed. Panel A: Size comparison of tumors from six mice of each group, BCG823 (top) and SGC7901 (bottom), with or without PGAM1 knockdown. Panel B: Tumor weights in each group at the end of the experiment. Panel C: Tumor growth kinetics (volume) in each group over the six week

time course. Panel D: Body weight comparison of mice in each cohort of mice. *<0.05, ***p<0.001, ****p<0.0001.

Supplementary Files

This is a list of supplementary files associated with this preprint. Click to download.

- WangetalsupplementalmaterialsCellularOncology2022.pdf